

Self-Nitrogen-Doped Biochar Derived from Soybean cake for Rhodamine B Removal Prepared via Simple Carbonization

Xinyu Zhang,^{a,b} Chao Yang,^a Tingwei Zhang,^a Jiaqi Guo,^a Yusheng Gan,^b Haibiao Wu,^b Mohammad Rizwan Khan,^c Huining Xiao,^d and Junlong Song^{a,*}

Nitrogen-doped biochar performs much better in dye adsorption due to its rich functional groups. Soybean cake, a by-product of soybean oil production, comprises rich contents of cellulose, lignin, and protein. Therein, simple direct carbonization was utilized to prepare self-nitrogen-doped biochar (SCB). The results showed that the N content of SCB was 6.81 wt%, and its specific surface area was 18.8 m²/g. X-ray photoelectron spectroscopic results confirmed that the surface of SCB was rich in pyridine-N, pyrrole-N, graphite-N, and oxidized-N functional groups. The adsorption capacity of SCB for Rhodamine B was 17.2 mg/g, which is higher compared with other unactivated biochars. The results of thermodynamic parameters indicate that Rhodamine B adsorption on SCB is an endothermic, entropy-increasing, and spontaneous process.

DOI: 10.15376/biores.18.4.7460-7473

Keywords: Soybean cake; Self-nitrogen-doped biochar; Rhodamine B; Adsorption; Thermodynamics

Contact information: a: Jiangsu Co-Innovation Center for Efficient Processing and Utilization of Forest Resources, Nanjing Forestry University, Nanjing 210037, China; b: Hangzhou HUAWON New Material Technology Co., Ltd, Hangzhou 311305, China; c: Department of Chemistry, College of Science, King Saud University, Riyadh 11451, Saudi Arabia; d: Department of Chemical Engineering, University of New Brunswick, Fredericton, NB, E3B 5A3, Canada; *Corresponding author: junlong.song@njfu.edu.cn

INTRODUCTION

Today, textile dyeing produces a large amount of dye wastewater. Since azo dyes are mutagenic, teratogenic, and carcinogenic (Chung 1983), they can cause severe damage to human health and the ecological environment if dye wastewater is not treated effectively or discharged directly (Al-Tohamy *et al.* 2022). Compared with membrane filtration and advanced oxidation processes, such as Fenton, electrocatalysis, ozone, and electrochemical oxidation (Albadarin *et al.* 2017; Boudissa *et al.* 2019; Crini and Lichtfouse 2019), adsorption is one of the most commonly used technologies to remove pollutants with small or medium molecular size in water since it is convenient, efficient, and inexpensive (Bushra *et al.* 2021). Among many adsorption materials, biochar is regarded as one of the most promising adsorbent materials because it has many excellent properties in respect of containing oxygen-containing functional groups, excellent stability, low cost, and easy availability (Goodman 2020).

Recently, the modification of biochar by nitrogen doping has attracted much interest, since the doped nitrogen on the surface of biochar enhances electron mobility and improves its hydrophobic properties (Kasera *et al.* 2022). As such, nitrogen-doped biochars perform much better in adsorbing heavy metals and organic chemicals (Yin *et al.* 2019).

Nitrogen-doping in biochar is usually carried out in two ways: one is self-nitrogen-doped biochar, which uses the biomass that is rich in N element as raw material to prepare biochar; the other is using exogenous nitrogen additive or exogenous nitrogen (post-processing strategy) (Wan *et al.* 2020). The typical nitrogen additives used in the post-processing strategy include inorganic substances and organic matter (Guo *et al.* 2019; Lian *et al.* 2016). Compared with the post-processing strategy, the self-nitrogen-doping method provides an easier way to bind nitrogen atoms into the carbon lattice of biochar, which can maintain a well-structured and evenly distributed nitrogen (Duan *et al.* 2015). In addition, the self-nitrogen-doping method involves simpler operations and avoids potentially harmful or expensive chemical agents (Gao *et al.* 2016).

Soybean cake (SC), a by-product of soybean oil production, is mainly used to feed animals. Along with rich cellulose and lignin, which can serve as carbon sources, SC contains rich protein (more than 42%) (Yuan *et al.* 2010); therefore, it is an excellent potential raw material for self-nitrogen-doped biochar fabrication. For instance, Yin *et al.* (2019) used SC to prepare the self-nitrogen-doped biochar (SCB), and the adsorption capacity for Pb^{2+} reached 133.6 mg/g. However, the physicochemical properties of organic pollutants, such as molecular structure and molecular weight (M_w), may greatly affect the adsorption performance of activated carbon (Ahmed and Hameed 2018). Therefore, the adsorption of small organic molecules, *e.g.*, dyes, by self-nitrogen-doped biochar still has excellent research prospects.

In this study, SC-derived self-nitrogen-doped biochars were prepared through direct carbonization at different temperatures (600, 700, and 800 °C) and characterized. Then the adsorption performance of SCB for Rhodamine B (RhB) was evaluated, and the adsorption kinetics and thermodynamic analysis were assessed.

EXPERIMENTAL

Materials

Soybean cake was acquired from Chaiji grain station (Fuyang, China). Rhodamine B (RhB, $M_w = 479.01$ g/mol, $\lambda_{\text{max}} = 554$ nm) was purchased from Aladdin Bio-Chem Technology Co., LTD (Shanghai, China). Ethanol (99.5 wt%) was supplied by Yasheng Chemical Co., LTD (Wuxi, China), HCl (36.7 wt%) and NaOH were provided by Sinopharm Chemical Reagent Co. Ltd. (China). All reagents were analytical grade and used as received.

Preparation of Adsorbents

To begin, SC powder was added into a ceramic ark and placed in a tubular furnace (Kejing, GSL-1100X-XX-S2). It was heated with a heating rate of 5 °C/min under 99.99% N_2 atmosphere and then kept at different temperatures (600, 700, and 800 °C) for 1 h. The pyrolytic residues were soaked in 2 mol/L HCl solution for several hours, then washed thoroughly using deionized water. Finally, the dry SCB adsorbents were obtained by drying the collected samples in an oven at 80 °C for 8 h.

The pre-experiment results showed that SCB prepared at 800 °C demonstrated the highest adsorption capacity for RhB; it was mainly due to the increase of pore volume and specific surface area caused by the removal of volatile organic compounds at a high temperature (Chen *et al.* 2008). The SCB used below was the sample prepared at 800 °C unless mentioned.

Characterizations

The details of the characterization methods are described in Appendix S1 (Supporting Information).

Adsorption Performance Test

Briefly, 100 mL of RhB solution was added into a 250 mL flask with an initial concentration of 1 to 10 mg/L. The pH of RhB solutions was adjusted to 2, 4, 6, 8, 10, and 12 with dropping HCl (0.1 mol/L) or NaOH (0.1 mol/L) solution. Approximately 200 mg SCB was added into each solution every time, and the adsorption time ranged from 1 to 720 min. During adsorption, all conical flasks were kept in an incubator shaker (ZWY-2101, Shanghai, China) at constant stirring (150 rpm). More information related to removal efficiency, adsorption capacity, adsorption kinetics, adsorption isotherm models, and thermodynamic analysis is addressed in detail in Appendix S2 & 3.

RESULTS AND DISCUSSION

Characterization of Adsorbent

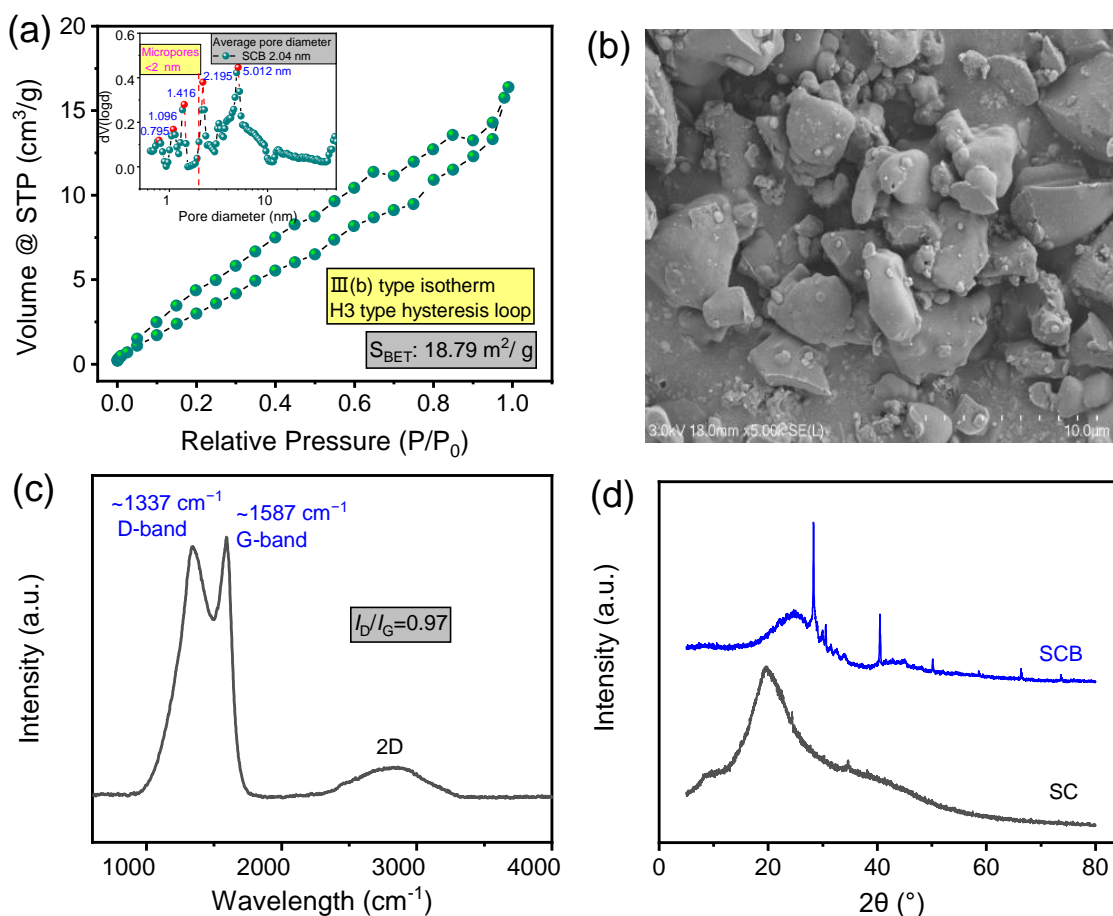


Fig. 1. N₂ adsorption-desorption isotherm and pore size distribution based on DFT model (a), SEM diagram (b), Raman spectra (c) of SCB, and XRD patterns of SC and SCB (d)

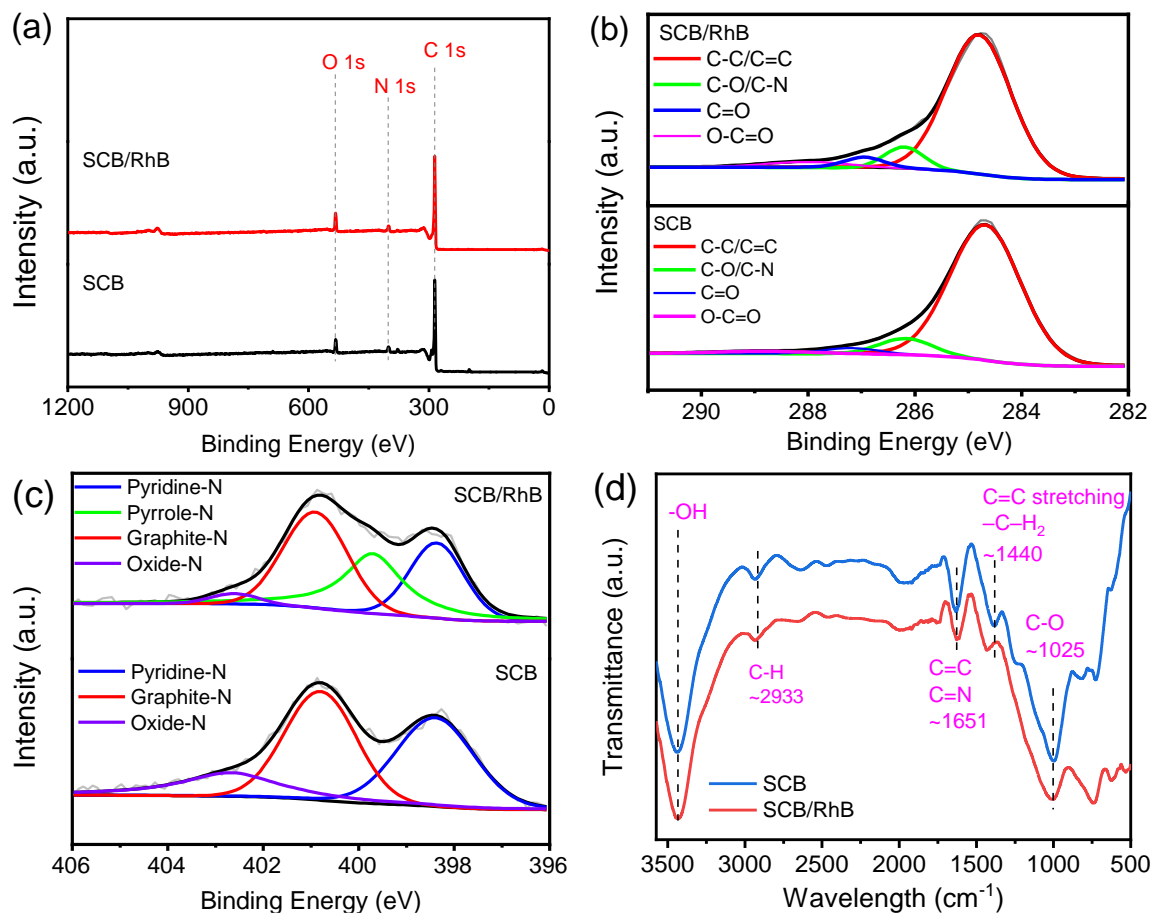


Fig. 2. XPS spectrum (a), C 1s (b), N 1s (c) for SCB and SCB/RhB, and FT-IR spectra of SCB and SCB/RhB (d)

The textural properties of SCB were characterized using a surface area analyzer (Quanta Chrome Nova 1200). Figure 1(a) shows the result for the N_2 adsorption-desorption isotherm, which was a III(b) type isotherm with H3 hysteresis loop, and the S_{BET} was 18.79 m^2/g obtained from the DFT model. According to the t -plot method, the external surface area was also 18.79 m^2/g , while the micropore surface area was negligible. The pore size distribution (insert in Fig. 1(a)) shows that SCB has few micropores or mesopores. This was also confirmed by the SCB pore volume of only 0.021 cm^3/g , and the dominant pore size was 5.39 nm. Figure 1(b) shows that SCB is depicted as some particles aggregates of different sizes with a relatively smooth and flat surface. The Raman spectrum of SCB is demonstrated in Fig. 1(c); two prominent diffraction peaks appear at 1337 and 1587 cm^{-1} , corresponding to the “D-band” and “G-band” of carbon materials, respectively. The disordered degree of carbon materials can be measured by the ratio of I_D/I_G . A higher I_D/I_G value indicates a higher defect degree and lower graphitization degree. The calculated I_D/I_G of SCB was 0.97. The 2D peak (~ 2705 cm^{-1}) is another characteristic peak of the graphite material, and the position and shape can be used to identify the stratification of carbon materials.

The XRD pattern of SC is displayed in Fig. 1(d). That pattern was similar to that of cellulose because cellulose contributes most to SC due to its crystalline structure. After carbonization, two distinct diffraction peaks at approximately 22.8° and 42.2° were

present, corresponding to the (002) and (101) crystallographic planes of graphitic carbon (Xiao *et al.* 2020). Similar XRD diffraction patterns of biochar derived from different precursors were also reported in the literature (Ho *et al.* 2019; Sevilla *et al.* 2011). It was also noted that some sharp peaks appeared at $2\theta = 28.3, 40.5, 47.8, 50.1, 58.6, 66.3,$ and 73.6° , which are due to the mineral potassium salts in the inorganic material (Pariyar *et al.* 2020). This indicates that the HCl solution cannot effectively remove impurities inside the biochar without activation. Thus, the remaining ash in SCB is high.

In addition, X-ray photoelectron spectroscopy (XPS) was employed to detect the chemistry changes on the adsorbent surface. Figure 2(a) shows that SCB is mainly composed of C, O, and N. Figure 2(b) shows several fitting peaks at 284.8, 285.8, 286.5, and 288.9 eV, which represent the C–C/C=C, C–O/C–N, C=O, and –COOH groups, respectively (Mena-Durán *et al.* 2018; Wu *et al.* 2020b). Figure 2(c) shows the N 1s spectrum, which can be deconvoluted into four peaks around 398.1 to 398.4 eV (pyridine-N), 399.1 to 400.5 eV (pyrrole-N and/or pyridine-N), 400.8 to 401.3 eV (graphite-N), and 402.8 eV (oxide-N) (Lian *et al.*, 2016). Pyridines and graphite-N were the main components of N-doped biochar, and the content of oxide-N is less. In Fig. 2(d), the broad bands of each sample at approximately 3450 cm^{-1} are due to either the water absorbed by the biochar or the stretching vibration peaks of –OH contained on the biochar surface. The characteristic peak was detected at $1690\text{ to }1590\text{ cm}^{-1}$, which is attributed to the stretching vibrations of the –C=C/ and C=N bonds, while peaks near 1440 and 1025 cm^{-1} are attributed to C=C stretching/–C–H₂ bending and symmetric C–O stretching or C–N stretching vibration, respectively (Chanajaree *et al.* 2021; Keiluweit *et al.* 2010). Oxygen-containing groups would be beneficial to electrostatic interaction and surface complexation between adsorbent and organic dyes. In addition, nitrogen content in SCB was 6.81 wt.% obtained by elemental analysis (Table S1), confirming it contains sufficient N content.

Adsorption Performance Experiments

Effect of pH on adsorption performance

Figure 3(a) shows the relationship between the initial pH of the adsorbent solution and the adsorption capacity of SCB. It can be seen that the adsorption capacity of SCB achieved its maximum at approximately pH = 6.0. When the pH of the solution is higher than 3.7 (the pK_a of RhB), RhB molecules change from cationic to zwitterion due to the deprotonation of the carboxyl group in RhB. When SCB interacts with RhB molecules, the positive charge causes electrostatic repulsion under pH < 6.2; whereas when pH > 3.7, RhB molecules may form dimers, thus affecting dye molecules' adsorption (Deng *et al.* 2019).

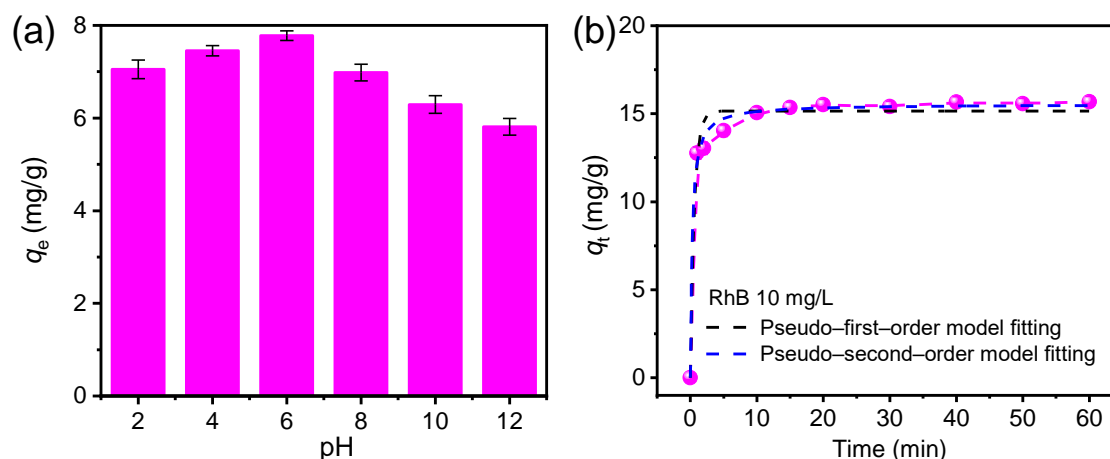


Fig. 3. Effects of pH (a) and adsorption time (b) on the adsorption capacity of SCB for RhB
Adsorption kinetic models fitting

Figure 3(b) shows the adsorption process of RhB on SCB over time. The adsorption process presents two stages (fast and slow adsorption). The fast adsorption rate in the early stage is due to the presence of a large number of adsorption sites on SCB. Subsequently, the adsorption rate decreases as adsorption progresses due to the decreasing number of sites on SCB surface and the decrease of adsorbate concentration in the solution (Wu *et al.* 2020). The results of the parameters are shown in Table 1. Regarding the fitting results, considering the values of R^2 are very close to 1, these two models can fit the experimental adsorption data well, especially the pseudo-second-order model.

Table 1. Parameters of Kinetics Model for RhB Adsorption on SCB

Pseudo-first-order Model			Pseudo-second-order Model		
R^2	k_1 (1/min)	q_e (mg/g)	R^2	k_2 (g/(mg·min))	q_e (mg/g)
0.9772	1.62	15.15	0.9935	0.2349	15.53

Adsorption isothermal models fitting

Figure 4(a) shows that the adsorption capacity of SCB for RhB increased with initial concentration and temperature. On the one hand, an increase in initial adsorbent concentration will lead to an increase in adsorbent capacity, possibly due to the significant driving force for mass transfer at a higher initial dye concentration; on the other hand, as the adsorption temperature increases, the mobility of dye molecules increases, and the number of adsorbable active sites also increases (Salleh *et al.* 2011).

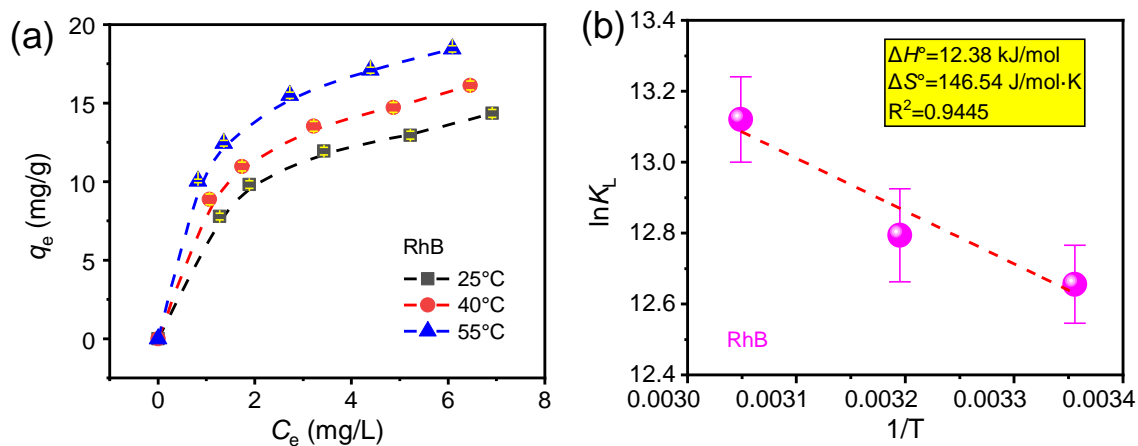


Fig. 4. Effect of temperature and concentration on the adsorption capacity (a), Function of $\ln K_L$ and $1/T$ of the adsorption rate constant of RhB on SCB (b)

Table 2. Parameters of Isotherm Model for RhB Adsorption on SCB

Temperature (°C)	Langmuir Isotherm Model			Freundlich Isotherm Model		
	q_m (mg/g)	K_L (L/mg)	R^2	K_F (mg/g)/(mg/L) ⁿ	$1/n$	R^2
25	17.25	0.65	0.9808	7.52	0.3424	0.9701
40	19.04	0.75	0.9929	8.95	0.3242	0.9870
55	21.16	1.04	0.9954	11.02	0.3000	0.9822

Table 2 shows the parameters of the isothermal models obtained by non-linear fitting. According to the Langmuir isotherm model fitting, the theoretical adsorption capacity of SCB for RhB at 25 and 55 °C was 17.25 and 21.16 mg/g, respectively. Compared with other adsorption materials reported in the literature, such as nosean composite (14.1 mg/g) (Ni *et al.* 2022), waste coconut shell biochar (12.41 mg/g) (Li *et al.* 2022), and Fe-N-biochar (12.4 mg/g) (Li *et al.* 2022), the adsorption capacity of SCB can be regarded as good enough.

The results of FT-IR and XPS show that the surface of SCB contains carboxyl, hydroxyl, and nitrogen-containing functional groups. Carboxyl and hydroxyl groups can form hydrogen bonds with hydroxyl groups on RhB molecules. In addition, the electrostatic adsorption between SCB and RhB cannot be ignored. Raman spectroscopy and XRD confirm that SCB has a graphite structure, RhB molecules are planar molecular structures, which can form π - π accumulation on the surface of biochar.

Ethanol desorption technology was used to evaluate the feasibility of reproducing SCB. The percentage of RhB desorption results is as high as 99%. Therefore, it can be considered that almost all adsorption points of SCB are recovered from the desorption process.

Adsorption thermodynamics

Figure 4(b) shows the fitting of adsorption thermodynamic parameters, and the fitting results are shown in Table 3. The ΔG° values of RhB adsorbed on SCB at multiple different temperatures were all negative, indicating that the adsorption was spontaneous in the system under a normal state (Fenti *et al.* 2019). Positive ΔH° values suggest that the adsorption of RhB on SCB is an endothermic process. Positive ΔS° values indicate that the

adsorption of RhB on SCB leads to increased disorder at the biochar/adsorbate solution interface.

Table 3. Thermodynamic Parameters Related to Adsorption of RhB on SCB

Temperature (K)	ΔG° (kJ/mol)	ΔH° (kJ/mol)	ΔS° (J/ (K·mol))
298	-31.35	12.38	146.54
313	-31.70		
328	-32.51		

CONCLUSIONS

1. In this study, soybean cake-derived SCB was successfully prepared through simple direct carbonization. Its specific surface area reached 18.8 m²/g and its nitrogen content was 6.81 wt.%.
2. According to Langmuir isotherm model fitting, the theoretical adsorption capacity of SCB for RhB reached 17.2 mg/g, which is relatively good for biochar prepared without any activation.
3. The ΔG° values were all negative, indicating that the adsorption of RhB on SCB was spontaneous; the positive ΔH° values indicate that the adsorption was endothermic; the positive ΔS° values indicate that the adsorption of dyes on SCB resulted in increased disorder at the biochar/adsorbate solution interface.

ACKNOWLEDGMENTS

This project was financially supported by the National Natural Science Foundation of China (Nos. 32101468 and 31770623), Natural Science Foundation of Jiangsu Province (No. BK20210622), Postgraduate Research & Practice Innovation Program of Jiangsu Province (SJKY19-0904), and the Priority Academic Program Development of Jiangsu Higher Education Institutions. M.R.K. acknowledged the Researchers Supporting Project (No. RSP2023R138), King Saud University, Riyadh, Saudi Arabia.

REFERENCES CITED

- Ahmed, M. J., and Hameed, B. H. (2018). "Adsorption behavior of salicylic acid on biochar as derived from the thermal pyrolysis of barley straws," *J. Clean. Prod.* 195, 1162-1169. DOI: 10.1016/j.jclepro.2018.05.257
- Al-Tohamy, R., Ali, S. S., Li, F., Okasha, K. M., Mahmoud, Y. A. G., Elsamahy, T., and Sun, J. (2022). "A critical review on the treatment of dye-containing wastewater: Ecotoxicological and health concerns of textile dyes and possible remediation approaches for environmental safety," *Ecotoxicol. Environ. Saf.* 231, 113160. DOI:10.1016/j.ecoenv.2021.113160
- Albadarin, A. B., Collins, M. N., Naushad, M., Shirazian, S., Walker, G., and Mangwandi, C. (2017). "Activated lignin-chitosan extruded blends for efficient

- adsorption of methylene blue," *Chem. Eng. J.* 307, 264-272. DOI: 10.1016/j.cej.2016.08.089
- Boudissa, F., Mirilà, D., Arus, V.-A., Terkmani, T., Semaan, S., Proulx, M., and Azzouz, A. (2019). "Acid-treated clay catalysts for organic dye ozonation-Thorough mineralization through optimum catalyst basicity and hydrophilic character," *J. Hazard. Mater.* 364, 356-366. DOI:10.1016/j.jhazmat.2018.09.070
- Bushra, R., Mohamad, S., Alias, Y., Jin, Y., and Ahmad, M. (2021). "Current approaches and methodologies to explore the perceptive adsorption mechanism of dyes on low-cost agricultural waste: A review," *Micropor. Mesopor. Mater.* 319, 111040. DOI:10.1016/j.micromeso.2021.111040
- Chanajaree, R., Sriuttha, M., Lee, V. S., and Wittayanarakul, K. (2021). "Thermodynamics and kinetics of cationic/anionic dyes adsorption on cross-linked chitosan," *J. Mol. Liq.* 322, article 114507. DOI:10.1016/j.molliq.2020.114507
- Chen, B., Zhou, D., and Zhu, L. (2008). "Transitional adsorption and partition of nonpolar and polar aromatic contaminants by biochars of pine needles with different pyrolytic temperatures," *Environ. Sci. Technol.* 42(14), 5137-5143. DOI:10.1021/es8002684
- Chung, K.-T. (1983). "The significance of azo-reduction in the mutagenesis and carcinogenesis of azo dyes," *Mutation Research/Reviews in Genetic Toxicology* 114(3), 269-281. DOI:10.1016/0165-1110(83)90035-0
- Crini, G., and Lichtfouse, E. (2019). "Advantages and disadvantages of techniques used for wastewater treatment," *Environ. Chem. Lett.* 17(1), 145-155. DOI:10.1007/s10311-018-0785-9
- Deng, H., Mao, Z., Xu, H., Zhang, L., Zhong, Y., and Sui, X. (2019). "Synthesis of fibrous LaFeO₃ perovskite oxide for adsorption of Rhodamine B," *Ecotoxicol. Environ. Saf.* 168, 35-44. DOI:10.1016/j.ecoenv.2018.09.056
- Duan, X., O'Donnell, K., Sun, H., Wang, Y., and Wang, S. (2015). "Sulfur and nitrogen co-doped graphene for metal-free catalytic oxidation reactions," *Small* 11(25), 3036-3044. DOI:10.1002/sml.201403715
- Fenti, A., Iovino, P., and Salvestrini, S. (2019). "Some remarks on 'A critical review of the estimation of the thermodynamic parameters on adsorption equilibria. Wrong use of equilibrium constant in the Van't Hoof equation for calculation of thermodynamic parameters of adsorption' - Journal of Molecular Liquids 273 (2019) 425-434," *J. Mol. Liq.* 276, 529-530. DOI:10.1016/j.molliq.2018.12.019
- Gao, Y., Xu, S., Yue, Q., Ortaboy, S., Gao, B., and Sun, Y. (2016). "Synthesis and characterization of heteroatom-enriched biochar from keratin-based and algous-based wastes," *Adv. Powder Technol.* 27(4), 1280-1286. DOI:10.1016/j.apt.2016.04.018
- Goodman, B. A. (2020). "Utilization of waste straw and husks from rice production: A review," *J. Bioresour. Bioprod.*, 143-162. DOI: 10.1016/j.jobab.2020.07.001
- Guo, S., Gao, Y., Wang, Y., Liu, Z., Wei, X., Peng, P., and Yang, Y. (2019). "Urea/ZnCl₂ *in situ* hydrothermal carbonization of *Camellia sinensis* waste to prepare N-doped biochar for heavy metal removal," *Environ. Sci. Pollut. Res. Int.* 26(29), 30365-30373. DOI:10.1007/s11356-019-06194-8
- Ho, S.-H., Chen, Y.-d., Li, R., Zhang, C., Ge, Y., Cao, G., and Ren, N.-q. (2019). "N-doped graphitic biochars from C-phycocyanin extracted *Spirulina* residue for catalytic persulfate activation toward nonradical disinfection and organic oxidation," *Water Res.* 159, 77-86. DOI:10.1016/j.watres.2019.05.008

- Kasera, N., Kolar, P., and Hall, S. G. (2022). "Nitrogen-doped biochars as adsorbents for mitigation of heavy metals and organics from water: A review," *Biochar* 4(1), 1-30. DOI:10.1007/s42773-022-00145-2
- Keiluweit, M., Nico, P. S., Johnson, M. G., and Kleber, M. (2010). "Dynamic molecular structure of plant biomass-derived black carbon (biochar)," *Environ. Sci. Technol.* 44(4), 1247-1253. DOI:10.1021/es9031419
- Li, X., Shi, J., and Luo, X. (2022). "Enhanced adsorption of rhodamine B from water by Fe-N co-modified biochar: Preparation, performance, mechanism and reusability," *Bioresour. Technol.* 343, 126103. DOI:10.1016/j.biortech.2021.126103
- Lian, F., Cui, G., Liu, Z., Duo, L., Zhang, G., and Xing, B. (2016). "One-step synthesis of a novel N-doped microporous biochar derived from crop straws with high dye adsorption capacity," *Journal of Environmental Management* 176, 61-68. DOI:10.1016/j.jenvman.2016.03.043
- Mena-Durán, C. J., Alonso-Lemus, I. L., Quintana, P., Barbosa, R., Ordoñez, L. C., and Escobar, B. (2018). "Preparation of metal-free electrocatalysts from cassava residues for the oxygen reduction reaction: A sulfur functionalization approach," *Int. J. Hydrogen Energy* 43(6), 3172-3179. DOI:10.1016/j.ijhydene.2017.12.139
- Ni, X., Sun, X., Xu, Y., and Xu, D. (2022). "A green and facile synthesis of nosean composite from coal fly ash for optimizing Rhodamine B adsorption using response surface methodology," *J. Mol. Liq.* 359, 119262. DOI:10.1016/j.molliq.2022.119262
- Pariyar, P., Kumari, K., Jain, M. K., and Jadhao, P. S. (2020). "Evaluation of change in biochar properties derived from different feedstock and pyrolysis temperature for environmental and agricultural application," *Sci. Total Environ.* 713, 136433. DOI: 10.1016/j.scitotenv.2019.136433
- Salleh, M. A. M., Mahmoud, D. K., Karim, W. A. W. A., and Idris, A. (2011). "Cationic and anionic dye adsorption by agricultural solid wastes: A comprehensive review," *Desalination* 280(1-3), 1-13. DOI: 10.1016/j.desal.2011.07.019
- Sevilla, M., Valle-Vigón, P., and Fuertes, A. B. (2011). "N-doped polypyrrole-based porous carbons for CO₂ capture," *Adv. Funct. Mater.* 21(14), 2781-2787. DOI:10.1002/adfm.201100291
- Wan, Z., Sun, Y., Tsang, D. C., Khan, E., Yip, A. C., Ng, Y. H., and Ok, Y. S. (2020). "Customised fabrication of nitrogen-doped biochar for environmental and energy applications," *Chem. Eng. J.* 126136. DOI:10.1016/j.cej.2020.126136
- Wu, J., Yang, J., Huang, G., Xu, C., and Lin, B. (2020). "Hydrothermal carbonization synthesis of cassava slag biochar with excellent adsorption performance for Rhodamine B," *J. Clean. Prod.* 251, 119717. DOI:10.1016/j.jclepro.2019.119717
- Wu, J., Yang, J. W., Huang, G. H., Xu, C. H., and Lin, B. F. (2020). "Hydrothermal carbonization synthesis of cassava slag biochar with excellent adsorption performance for Rhodamine B," *J. Clean. Prod.* 251. DOI: 10.1016/j.jclepro.2019.119717
- Xiao, W., Garba, Z. N., Sun, S., Lawan, I., Wang, L., Lin, M., and Yuan, Z. (2020). "Preparation and evaluation of an effective activated carbon from white sugar for the adsorption of rhodamine B dye," *J. Clean. Prod.* 253, 119989. DOI: 10.1016/j.jclepro.2020.119989
- Yin, W., Dai, D., Hou, J., Wang, S., Wu, X., and Wang, X. (2019). "Hierarchical porous biochar-based functional materials derived from biowaste for Pb(II) removal," *Appl. Surf. Sci.* 465, 297-302. DOI:10.1016/j.apsusc.2018.09.010

Yuan, S., Zhou, Z.-j., Li, J., Chen, X.-l., and Wang, F.-c. (2010). "HCN and NH₃ released from biomass and soybean cake under rapid pyrolysis," *Energy Fuels* 24(11), 6166-6171. DOI:10.1021/ef100959g

Article submitted: July 10, 2023; Peer review completed: July 26, 2023; Revised version received and accepted: August 21, 2023; Published: September 15, 2023.
DOI: 10.15376/biores.18.4.7460-7473

APPENDIX

Appendix S1: Characterization Methods

The surface morphology was visualized through a scanning electron microscope (SEM, JSM-7600F). The textural properties of biochar were evaluated via N₂ adsorption-desorption experiments using a surface area analyzer (Quantachrome Nova 1200), the degassing conditions for N₂ were under 200 °C for 4 h. The specific surface area (S_{BET}) was calculated by using the Brunauer-Emmett-Teller (BET) equation, and the pore diameter was calculated by using the density functional theory model. The crystalline structure and diffraction patterns of the samples were analyzed through X-ray diffraction (XRD, Rigaku Ultima IV) at a scan rate of 10°/min. The functional groups of the samples were analyzed by Fourier transform infrared reflection (FT-IR, VERTEX 80 V). The surface compositions of samples were determined on an X-ray photoelectron spectrometer (XPS, Ultra DLD) fitted with a hemispherical analyzer and a conventional monochromatic Al Ka X-ray source.

Appendix S2. Definition of Removal Efficiency and Adsorption Capacity

The model dyes removal efficiency and adsorption capacity at time t (q_t), are two crucial parameters for determining the adsorption capability of adsorbent, as defined by Equations. (S1 & S2), respectively.

$$\text{Removal efficiency} = \frac{(C_0 - C_t)}{C_0} \times 100\% \quad (\text{S1})$$

$$q_t = \frac{v(C_0 - C_t)}{m} \quad (\text{S2})$$

where C_0 (mg/L) denotes the initial concentration of adsorbate; C_t (mg/L) represents the residual concentration of adsorbate at time t ; q_t (mg/g) represents the adsorption capacity of adsorbate at time t ; v (L) denotes the volume of adsorbate solution; m (g) denotes the weight of adsorbent.

Appendix S3. Models Fitting and Thermodynamic Parameters

S3.1. Adsorption kinetics

For the kinetics study, the adsorbent was mixed with a series of adsorbate solutions and then shaken for different designed times. Various kinetic models have been used in the literature (Bedin *et al.* 2016; Wu *et al.* 2020b). In this paper, the adsorption kinetics was studied by pseudo-first-order and pseudo-second-order kinetics models. The parameters for these models were calculated using Eqs. S3 & S4, respectively.

$$q_t = q_e [1 - \exp(-k_1 t)] \quad (\text{S3})$$

$$q_t = \frac{k_2 q_e^2 t}{1 + k_2 q_e t} \quad (\text{S4})$$

where q_t represents the amount of dye adsorbed at time t (mg/g), and k_1 (1/min) and k_2 (g/mg·min) are the adsorption rate constants for pseudo-first-order and pseudo-second-order, respectively.

S3.2. Adsorption isotherms

The interactive behavior between solute and adsorbent in solution is usually described by equilibrium adsorption isotherms. The nonlinear equilibrium relationship between the solute adsorbed onto the adsorbent and that left in the solution can be explained by isotherm models. Herein, the adsorption data was studied in terms of the Langmuir and Freundlich isotherm models. Equations S5 and S6 express the non-linear of Langmuir isotherm and Freundlich isotherm (Wu *et al.* 2020a), respectively.

$$q_e = \frac{q_m K_L C_e}{1 + K_L C_e} \quad (S5)$$

$$q_e = K_f C_e^{\frac{1}{n}} \quad (S6)$$

where C_e (mg/L) means the residual concentration of dye in the solution at equilibrium; q_m (mg/g) is the maximum value of q_e and it varies with C_e ; K_L (L/mg) is a constant related to the affinity between an adsorbent and adsorbate; K_f (mg/g)/(mg/L) $^{\frac{1}{n}}$ is the Freundlich constant, and n (dimensionless) is the Freundlich intensity parameter, which indicates the magnitude of the adsorption driving force or the surface heterogeneity.

S3.3. Thermodynamic analysis

The thermodynamic parameters associated with adsorption, such as Gibbs free energy changes (ΔG°), standard enthalpy changes (ΔH°), and standard entropy changes (ΔS°), can be assessed by Eqs. (S7 to S9) (Liu *et al.* 2020). Measuring the temperature dependence of K_L over a wide temperature range creates an opportunity to calculate the ΔH° and ΔS° of the investigated chemical process according to the van't Hoff equation via a non-linear parameter estimation.

$$\Delta G^\circ = -RT \ln K_L \quad (S7)$$

$$\ln K_{eq} = \frac{-\Delta H^\circ}{RT} + \frac{\Delta S^\circ}{R} \quad (S8)$$

$$\Delta G^\circ = \Delta H - T\Delta S^\circ \quad (S9)$$

where T (K) is the absolute temperature at which adsorption is carried out, R is the gas constant (8.314 J/K·mol), and K_{eq} is the dimensionless equilibrium constant that is numerically equal to the K_L obtained at a different temperature from the Langmuir adsorption isotherm model, and C_p is heat capacity (J/mol).

Table S1. Results of Elemental Analysis for Soybean Cake and Biochar

Sample	C (wt%)	H (wt%)	S (wt%)	N (wt%)
SC	47.25	6.67	0.16	7.12
SCB	66.99	1.25	0.07	6.81

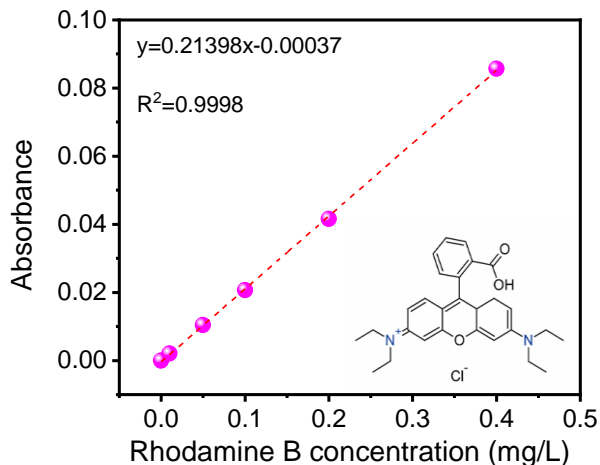


Fig. S1. The standard curve and structure of Rhodamine B

References Cited (Appendix)

- Bedin, K. C., Martins, A. C., Cazetta, A. L., Pezoti, O., and Almeida, V. C. (2016). "KOH-activated carbon prepared from sucrose spherical carbon: Adsorption equilibrium, kinetic and thermodynamic studies for Methylene Blue removal," *Chem. Eng. J.* 286, 476-484. DOI: 10.1016/j.cej.2015.10.099
- Liu, T., Zhang, Y., Lu, X., Wang, P., Zhang, X., Tian, J., and Xiao, H. (2020). "Binding affinity of family 4 carbohydrate binding module on cellulose films of nanocrystals and nanofibrils," *Carbohydr. Polym.* 251, 116725. DOI: 10.1016/j.carbpol.2020.116725
- Wu, J., Yang, J., Feng, P., Huang, G., Xu, C., and Lin, B. (2020). "High-efficiency removal of dyes from wastewater by fully recycling litchi peel biochar," *Chemosphere* 246, 125734. DOI: 10.1016/j.chemosphere.2019.125734
- Wu, J., Yang, J., Huang, G., Xu, C., and Lin, B. (2020). "Hydrothermal carbonization synthesis of cassava slag biochar with excellent adsorption performance for Rhodamine B.," *J. Clean. Prod.* 251, 119717. DOI: 10.1016/j.jclepro.2019.119717